



**HAL**  
open science

## Some aspects of wind-wave coupling at high winds

Jean-Paul Giovanangeli, Nicolas Reul, Marie Helene Garat, Hubert Branger

► **To cite this version:**

Jean-Paul Giovanangeli, Nicolas Reul, Marie Helene Garat, Hubert Branger. Some aspects of wind-wave coupling at high winds. S. G. Sajjadi; N. H. Thomas; J. C. R. Hunt. Wind-over-Wave couplings. Perspectives and Prospects, 69, Clarendon Press; Oxford University Press, pp.81-90, 1999, Institute of Mathematics and its Applications Conference Series, 9780198501923. hal-00192505

**HAL Id: hal-00192505**

**<https://hal.science/hal-00192505>**

Submitted on 17 May 2023

**HAL** is a multi-disciplinary open access archive for the deposit and dissemination of scientific research documents, whether they are published or not. The documents may come from teaching and research institutions in France or abroad, or from public or private research centers.

L'archive ouverte pluridisciplinaire **HAL**, est destinée au dépôt et à la diffusion de documents scientifiques de niveau recherche, publiés ou non, émanant des établissements d'enseignement et de recherche français ou étrangers, des laboratoires publics ou privés.



Distributed under a Creative Commons Attribution 4.0 International License

# Some Aspects of Wind-Wave Coupling at High Winds: an Experimental Study

J.P. Giovanangeli, N. Reul, M.H. Garat and H. Branger

*Institut de Recherche sur les Phénomènes Hors Equilibre, Laboratoire IOA, Marseilles, France*

## Abstract

Experiments were conducted in the IRPHE wind-wave facility in order to study the evidence and occurrence of air-flow separation above short wind waves. An original air-flow separation probe was designed and a Particle Image Velocimetry (PIV) technique in the air close to the surface was carried on. Measurements above steep waves clearly show air-flow separation at the crest, organised vortex motions with reverse flow above the leeward face and reattachment on the windward face of the downstream wave. Occurrence of air-flow separation grows linearly with wave steepness and decreases with wave age. The associated effects on wind-wave coupling are investigated.

## 1 Introduction

Momentum and energy fluxes from wind to waves are still not well understood, more particularly at high winds. This is due to the lack of knowledge on the structure of pressure and velocity fields in the close vicinity of steep and breaking waves. Some authors ([1, 2, 3, 4, 5, 6, 7]) argued that over steep laboratory wind waves, air-flow separation (AFS) could occur leading to significant changes on the wind-wave coupling and on the momentum and energy fluxes between air and water flows. However, as mentioned in [8], the results concerned a particular range of laboratory wind waves or quasi-steady breaking waves. No direct observations of the spatial structure of the air flow in the close vicinity of short wind-forced steep gravity waves were systematically done.

This paper reports upon a complete series of experiments conducted in the large IRPHE wind-wave tank in order to study the structure of air flow above short and steep wind-forced waves. First we developed an original method capable to detect systematically the occurrence of air-flow separation at the wave crest and to quantify its effects upon momentum and energy fluxes from wind to wave. Then, we used a new and powerful method based upon air-flow visualisation technique: the Particle Imaging Velocimetry (PIV). The results show

definitely the occurrence of AFS process, its dependence on sea state and its significant effects upon the structure of the turbulent boundary layer and wind-wave coupling. These results are of crucial importance to modelize and to parametrize wind-wave interactions particularly for young seas.

## 2 Experimental procedures

A first series of experiments have been conducted in the large IRPHE wind-wave tank (60 m long, 3 m wide and 3 m high) described in details by [9]. A second series using PIV have been conducted in the  $(1/5)^{th}$  scale model of the large facility. A sophisticated experimental set-up has been used. It consisted in a) three capacitive wave gauges allowing to determine amplitudes, along-wind and cross-wind slopes of the waves; b) an original pressure probe developed at IRPHE to measure the air static-pressure fluctuations [10]; c) an X-wire to determine longitudinal and vertical turbulent wind velocity fluctuations; and d) a wave follower to locate the probes at a constant height above the instantaneous water surface in presence of waves. Some experiments have been done over combination of paddle and wind waves. For these runs, particular attention was taken in order to avoid parasitical noise induced by the paddle displacements. The procedure is described in details in [11].

A key part of the investigation was to develop an original method to detect systematically reverse upstream flow above the water surface induced by AFS as observed by [4] and [12]. The second one was to operate the PIV visualisation technique in order to give the spatial and temporal features of the air flow in the close vicinity of the waves.

### 2.1 The air-flow separation probe

Starting from the idea that AFS can induce reverse flow very close to the leeward face of the wave [12], the AFS probe detector consisted in two DANTEC R11 cylindrical films separated 0.3 mm apart in the mean wind direction. The cold film was located upstream the hot film. Finally, the two films were mounted on a wave follower to explore the air flow in the close vicinity of the water surface in presence of waves and particularly in the troughs. In absence of AFS, the air flow is flowing downstream, the thermal wake of the hot film is driven downstream and then the upstream cold wire does not detect any air-flow temperature fluctuation. On the other hand, if AFS occurs, it could generate upstream local recirculations, and then locally the cold film will detect a temperature fluctuation due to the thermal wake of the downstream hot film. The efficiency of the method has been proved by a complete series of tests in [13].

## 2.2 The PIV method

The air flow above unsteady breaking waves was measured with a particle image velocimetry system based on the cross-correlation technique. Unsteady breaking waves were generated at a fixed location in the  $(1/5)^{th}$  scale model of the large facility by focussing packet of waves generated by a wavemaker and forced by the wind. A 12 mJ doubled pulsed Nd:YAG laser was used to provide a light sheet about 1 mm thick directed downward at the measurements site. The air-flow was seeded with water particles with diameters about  $10 \mu m$ . Images of these illuminated particles were captured with a 80C42 DoubleImage 700 Dantec camera using a high-performance progressive scan interline CCD chip. The effective resolution of the CCD camera was of 768 (horizontal) x 484 (vertical) pixels. The camera and the light sheet were slightly inclined at  $10^\circ$  in order to detect the free surface. Flow above wave groups were then analysed with the Dantec Flowmap Processor for different wind speeds, wave group amplitudes and breaking point positions.

## 3 Results and discussions

First we studied the statistical link between the structure of the turbulent air flow and the water surface displacements. We investigated the evolution with height of the coherency function between along-wind wave slope and the static pressure fluctuations in the air for different wind velocities. As expected, for a given mean wind velocity, the coherency function decreases as the height increases but for a given height, the coherency increases as the mean wind increases. This suggests here that larger is the wind higher is the coupling between the air flow and the waves.

Usually it is assumed that the exponential decay in amplitude with the height of the wave-induced fluctuations evolves as  $e^{-\alpha k z}$  with  $\alpha$  a decay parameter taken as a constant close to the unity and  $k$  the wavenumber of the wave. By measuring the evolution with height of the correlation function between air-pressure fluctuations and longitudinal wave slope, we estimated the vertical evolution of the amplitude of wave-induced pressure fluctuations. The decay coefficient  $\alpha$  was found to be wave-age dependent. The coefficient is close to 1.5 and decreases as the wave age decreases. This result suggests again that wind-wave coupling increases as the wave age decreases, as predicted by others [14, 15].

To quantify the wind-wave coupling, we determined the contribution of wave-induced organised motions to the total stress for different sea states. This was done by others [15, 16], considering the ratio  $\tau_w/\tau$  where  $\tau_w$  is the wave-induced stress and  $\tau = \rho u^{*2}$  is the total stress. In this work, the organised wave-induced stress has been considered by comparison between the form drag (correlation  $(p'\eta_x)_{z=\eta}$  between pressure fluctuations  $p'$  at the surface and longitudinal wave slopes  $\eta_x$ ) and the total stress  $\tau$ . As it was not possible to measure directly the air-pressure fluctuation at the water surface, the form drag  $(p'\eta_x)_{z=\eta}$  was estimated at the height  $z$  and extrapolated at  $z = \eta$ , taking into account the

decay coefficient value  $\alpha$  as a function of wave age  $c/u^*$ . The contribution of the wave-induced motions to the total stress is not constant but depends upon the wave age as shown in Figure 1. One can observe that the ratio  $(p'\eta_z)_{z=\eta}/\tau$ , which can be considered as a wind-wave coupling parameter, is maximum close to  $c/u^* = 2$ , for example, for young gravity waves. This is consistent with results obtained by others [12, 16, 17, 18]. We can observe that for older gravity waves ( $c/u^* > 3$ ) the wind-wave coupling parameter decreases as the wave age increases and tends to reach the value of 20% which is in agreement with [19] and [20]. Finally, for very young waves the contribution of the form drag to the total stress decreases. This suggest that for these waves the viscous stress takes a prominent part to support momentum flux from wind to waves.

Now the question arises: why wind-wave coupling by means of coherent pressure fluctuations increases as the wave age of gravity waves decreases? The structure of the velocity and pressure fields in the air flow has been investigated by using the AFS probe detector simultaneously with the pressure probe, hot-wire anemometers and wave gauges. Figure 2 displays the frequency of occurrence of

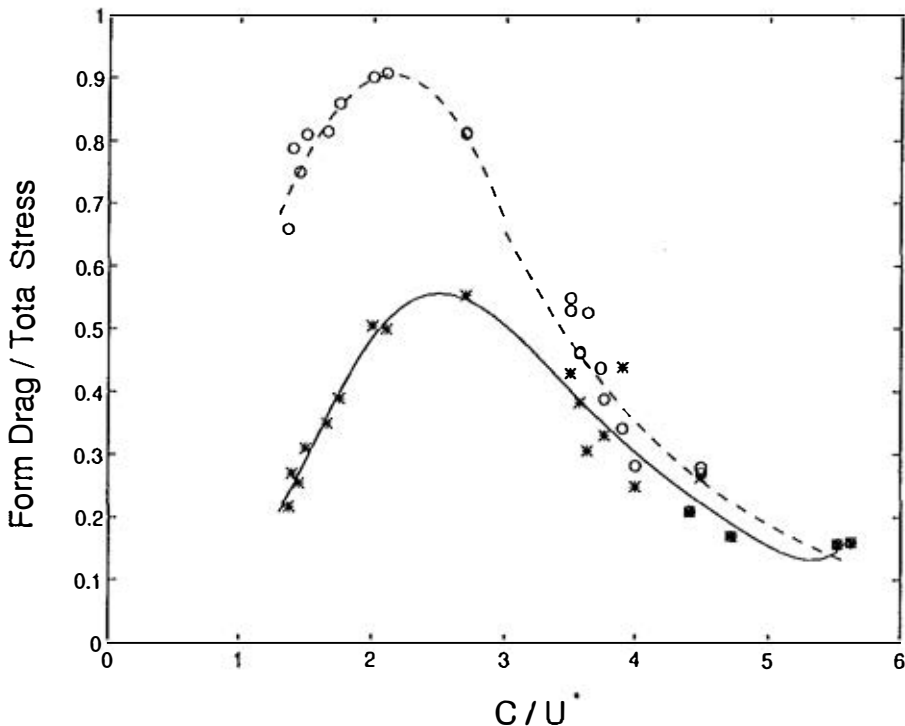
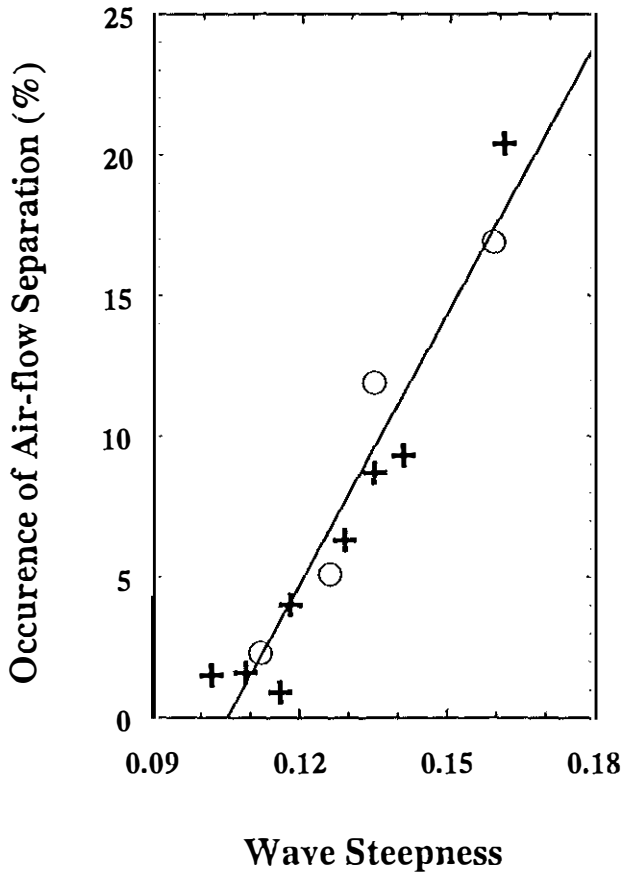


Figure 1. Contribution of the form drag to the total stress as a function of wave age  $c/u^*$  ( — waves without air-flow separation; - - - total wavefield)

AFS as a function of the wave steepness. The AFS occurrence increases linearly with the wave steepness and can reach 24% of the observed waves for a steepness of the dominant waves equal to 0.18. Figure 3 shows that the percentage of AFS occurrence, which is maximum for young gravity waves, decreases with the wave age of the dominant wave, and evolves as  $(c/u^*)^{-2.65}$ .



**Figure 2.** Occurrence (in %) of air-flow separation as function of wave steepness. (○ wind waves; + wind waves plus paddle waves)

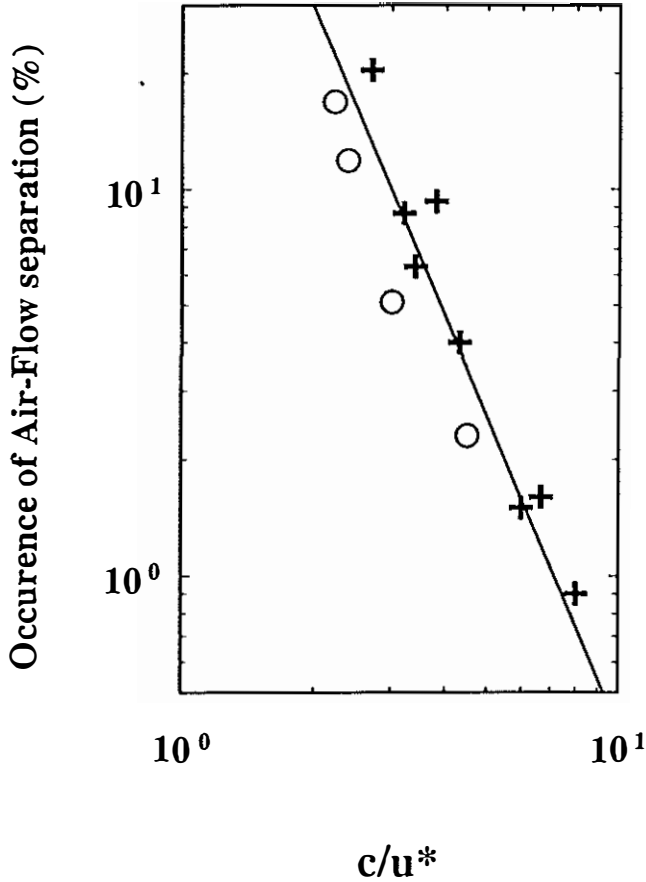
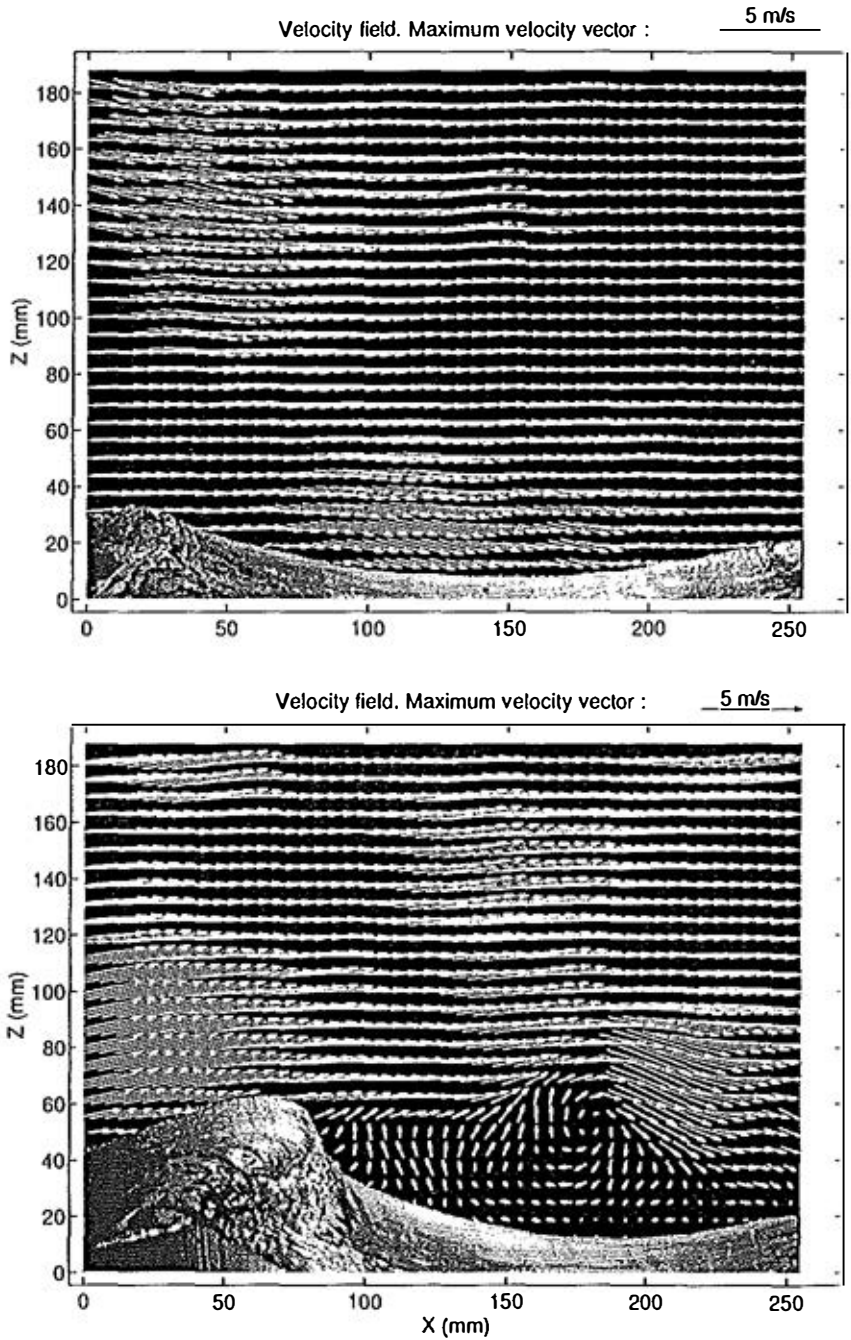


Figure 3. Occurrence (in %) of air-flow separation as function of wave age. (○ wind waves; + wind waves plus paddle waves)

Finally we found that the AFS process induces large spikes on the instantaneous product  $p'\eta_z$  just behind the highest crest and on the instantaneous product  $u'w'$  in phase with the trough of the highest wave. This seems to be in accordance with AFS which induces a reattachment point shifted in the downwind direction from the separation point located close to the highest wave crest. To consider the effects of AFS process upon the wind-wave coupling, conditional sampling have been applied to each  $u'$   $w'$   $p'$  and  $\eta_z$  time series. Data corresponding to the cases where AFS occurs and where AFS does not occur

have been considered separately. Figure 1 presents the evolution of the wind-wave coupling parameter  $(p'\eta_x)_{z=\eta} / \tau$ , as a function of the wave age with and without considering AFS. This figure shows clearly the role played by AFS in the wind-wave coupling. One can observe that the effect of AFS is maximum for  $c/u^*$  close to 2 and the form drag is increased by a factor of two when AFS occurs. The wind-wave coupling parameter is largely enhanced by the AFS. Nevertheless one can note that detection of AFS has been done here on the criterion of occurrence of reverse flow above the leeward face of the waves. This seems highly selective and one can argue that the measured AFS occurrence could be underestimated.

In order to verify definitely the existence of AFS another series of experiments have been conducted in the  $(1/5)^{th}$  scale model of the large wind-wave tank. In this set of experiments the Particle Imaging Velocimetry method described above has been operated. Figure 4 presents examples of PIV air-flow measurements. Above the steeper wave instantaneous wind-speed vectors processed by PIV clearly proves the occurrence of air-flow separation downwind the crest. When AFS occurs, PIV picture shows a) accelerated flow over the crest, b) well organised vortex motions with reverse flow above the leeward face, and c) reattachment on the windward face of the downstream wave. Data acquisition of  $p' u'$  and  $w'$  have been done simultaneously, and we project to correlate the occurrence of AFS observed by PIV with changes in momentum and energy fluxes over steep or breaking waves. Organised vortex motions on the leeward face of the waves could explain why the contribution of form drag to total stress increases as wave steepness increases. AFS should be taken into account to modelize wind-wave coupling. PIV results show that the water surface should not be considered as a streamline function as it is supposed in theoretical present models. Finally AFS suggests to not consider the existence of a constant shear layer in the close vicinity of the surface waves as it has been argued by others [19, 21].



**Figure 4.** PIV measurements above waves; top: without significant air-flow separation; bottom: evidence of air-flow separation with accelerated flow and coherent vortex motions

## 4 Conclusion and prospectives

Evidence of the occurrence of air-flow separation (AFS) process over wind waves has been proved by means of a series of experiments conducted in a large wind-wave tank. This has been done by using an original AFS detection probe and a PIV visualisation technique. The occurrence of the AFS grows linearly with the wave steepness and decreases as  $(c/u^*)^{-2.65}$ . Contrarily to the classical point of view, AFS could occur for relatively large values of  $c/u^*$ . As the effects of AFS is concerned, it has been shown that the AFS can induce well organised vortex motions above the leeward face of steep, near-breaking or breaking waves. The measured frequency of occurrence can reach 24% of the observed waves and can increase the contribution of the form drag to the total stress by a factor 2. For young gravity waves, corresponding to the maximum of occurrence of AFS, the form drag can represent about 80% of the total stress. This result has to be taken into account for new approaches to modelize momentum and energy fluxes over wind waves. Finally, close to the surface, the influence of waves appears as a fundamental process not only over the mean wind profile but also on the structure of the turbulent air flow. The question which arises now is to study the stability of the organised vortex motions generated by the AFS and particularly to compare their celerity of advection with the group and phase velocity of the underlying surface waves. The analysis of the data obtained by the PIV method are at present time analysed.

## 5 Acknowledgements

This work was supported by Grants ONR 14-93, DRET 94-147, CNRS/PATOM 91-1231 and ATP/PATOM 96-423.

## Bibliography

1. Wu, J. (1969). *Tellus*, **21**, 707–713.
2. Banner, M.L. and Melville, W.K. (1976). *J. Fluid Mech.*, **77**, 825–842.
3. Melville, W.K. (1977). *J. Phys. Ocean.*, **7**, 702–710.
4. Kawai, S. (1982). *Bound. Layer Met.*, **21**, 93–104.
5. Kawamura, H. and Toba, Y. (1988). *J. Fluid Mech.*, **197**, 105–138.
6. Bandou, T. and Mitsuyatsu, H. (1988). *Applied Mechanics*, **XXXV**, **104**, 13–34.
7. Banner, M.L. (1990). *J. Fluid Mech.*, **211**, 463–495.
8. Melville, W.K. (1996). *Ann. Review Fluid. Mech.*, **28**, 279–321
9. Favre, A. and Coantic, M. (1974). *Adv. Geophys.*, **18A**, 391–405.

10. Giovanangeli, J.P. (1988). *Experiments in Fluids*, **4**, 156–164.
11. Mastenbroek, C., Makin, V., Garat, M.H. and Giovanangeli, J.P., (1996). *J. Fluid Mech.*, **318**, 273–302.
12. Csanady, G.T. (1985). *J. Phys. Ocean.*, **15**, 1486–1494.
13. Garat, M.H. (1995). Ph D., *Thèse de Doctorat*. Université de la Méditerranée.
14. Makin, V. (1988). *Morshoy Gidnofizichesky Zhurnal*, **2**, 55–64.
15. Burgers, G. and Makin, V. (1993). *J. Phys. Ocean.*, **23**, 372–385.
16. Hsu, C.T., Wu, H.Y., Hsu, E.Y. and Street, R.L. (1982). *J. Phys. Ocean.*, **12**, 929–951.
17. Papadimitrakis, Y.A., Hsu, E.Y., and Street, R.L. (1984). *J. Fluid Mech.*, **170**, 113–137.
18. Weber, S.L. (1993). *J. Phys. Ocean.*, **24**, 1388–1398.
19. Janssen, P.A. (1989). *J. Phys. Ocean.*, **19**, 745–754.
20. Makin, V. (1990). *Atmos. Ocean. Phys.*, **26**, 434–439.
21. Belcher, S.E. and Hunt, J.C. (1993). *J. Fluid Mech.*, **251**, 109–148.